Electronic Supplementary Material (ESI) for Nanoscale.

Ultrahigh electron mobility induced by strain engineering in directly semiconducting monolayer Bi_2TeSe_2

Supplementary

Zixuan Lu,[1] Yu Wu,[2] Yuanfeng Xu,[3] Congcong Ma,[1] Ying Chen,[1] Ke Xu,[2] Hao Zhang,[2,*] Heyuan Zhu,[2] and Zhilai Fang[1,†]

[1]Academy for Engineering and Technology, Fudan University,
and Engineering Research Center of Advanced Lighting Technology,
Ministry of Education, Shanghai 200433, China

[2]Key Laboratory for Information Science of Electromagnetic Waves
(MOE) and Department of Optical Science and Engineering and
Key Laboratory of Micro and Nano Photonic Structures (MOE),
Fudan University, Shanghai 200433, China

[3]School of Science, Shandong Jianzhu University, Jinan 250101,China

I. 2D STRUCTURE PREDICTION USING THE PARTICLE SWARM OPTIMIZATION METHOD

We use the particle swarm optimization (PSO) method within the evolutionary algorithm implemented in the Crystal structure AnaLYsis by Particle Swarm Optimization (CALYPSO) code[1,2], to conduct the global structure search for the global energy-minimum structure of the stoichiometric monolayer Bi_2TeSe_2. The unit cell containing two Bi atoms, one Te atom and two Se atoms is considered, and three sublayers with a vacuum gap of 30Å are set as the parameters for 2D structure prediction. In the first step, 20 random structures with certain crystal symmetry are constructed, in which the atomic coordinates are generated by the crystallographic symmetry. Then, we use VASP code to carefully optimize the random structures until the Gibbs free energy changes are smaller than 1×10^{-5} eV. After finishing the structural optimization of all 20 random structures, 60% of them with lower Gibbs free energies are selected to partially construct the next-generation of PSO. The rest 40% new structures of the next-generation PSO are generated based on the so-called structure fingerprinting technique of bond characterization matrix to avoid identical structures[2]. In the case of monolayer Bi_2TeSe_2, the structure searching simulations stop at 10 generations and 200 structures are generated and under investigations. The information about the ten structures with lowest formation enthalpies is listed as Table S1.

TABLE S1: Ten structures with lowest formation enthalpies predicted by the PSO method.

No.	1	2	3	4	5	6	7	8	9	10
Symmetry(Group)	Pmm2(25)	P-3m1(164)	R3m(160)	P-3m1(164)	R3m(160)	R3m(160)	Fm2m(42)	P3m1(156)	P1(1)	P1(1)
Enthalpy (eV)	-4.32352	-3.88476	-3.88332	-3.88113	-3.88065	-3.87994	-3.87106	-3.83183	-3.74489	-3.73646

The ten structures with lowest formation enthalpies are shown in Table S1. The structure with the symmetry of Pmm2 as shown in Fig. S1(a) and the most lowest formation enthalpy predicted by CALYPSO as shown in Table S1, composes of three isolated monolayers with large distances between each other, so it is invalid and we neglect this structure. The second structure possesses the crystal symmetry of P-3m1, and it is shown in Fig. S1(b). By comparison, we find that, the second structure shown in Fig. S1(b) is the monolayer Bi_2TeSe_2 we predicted by the atomic transmutation method in the present work.

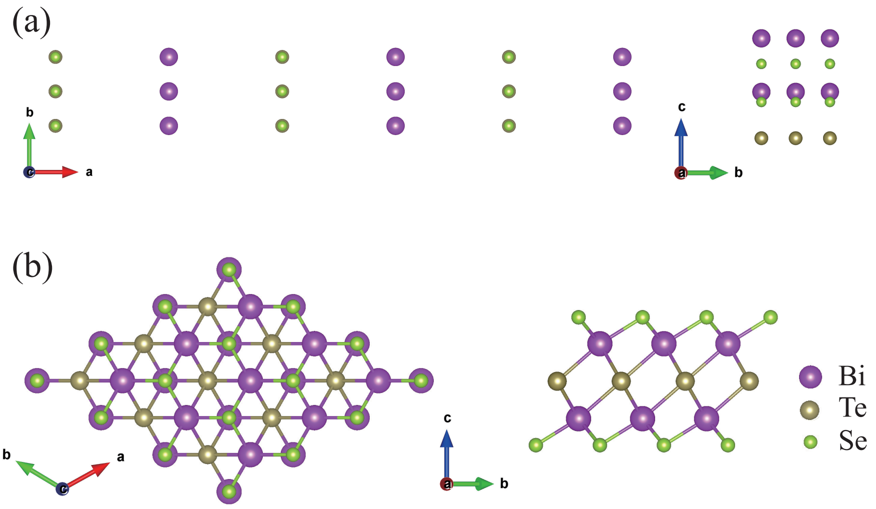

FIG. S1: Two predicted structures with lowest formation enthalpies, corresponding to (a) No. 1 and (b) No. 2 in Table S1.

II. VDW CORRECTIONS TO THE BAND STRUCTURES, OPTICAL PROPERTIES AND CARRIER MOBILITIES

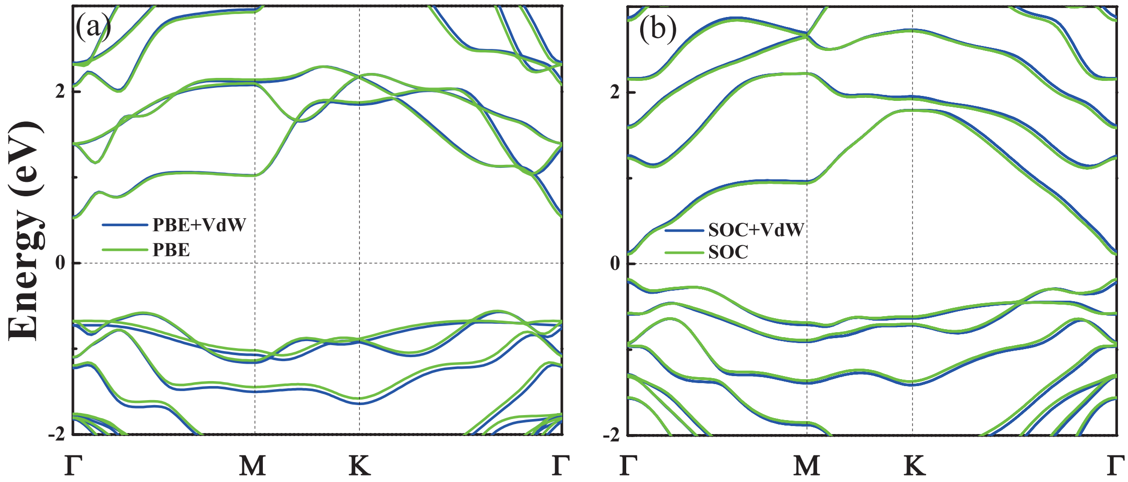

FIG. S2: Electronic band structures of monolayer Bi_2TeSe_2 calculated at the (a) PBE (b) PBE+SOC levels with/without vdW interaction.

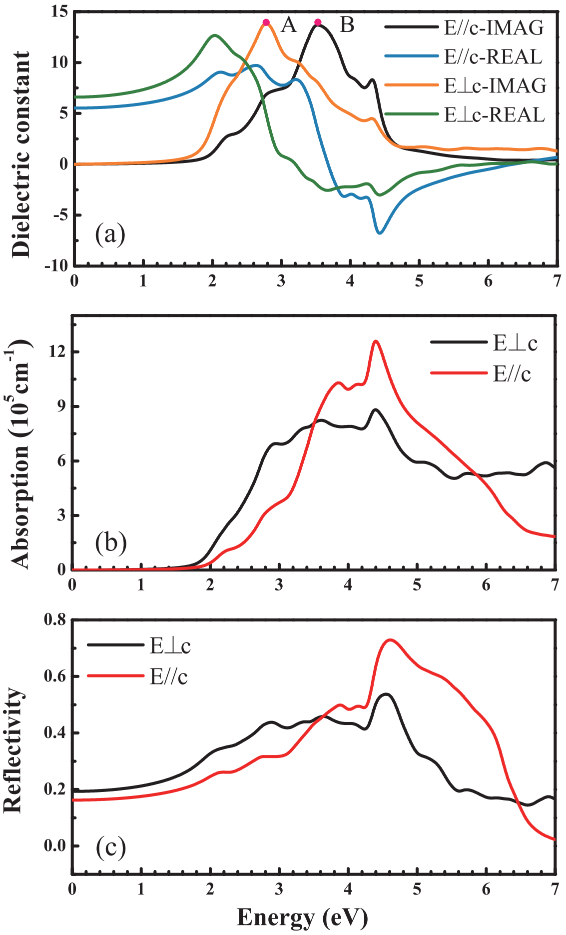

FIG. S3: Calculations of (a) dielectric functions for in-plane polarization (E⊥c) and out-of-plane polarization (E//c), (b) absorption coefficients, (c) reflectivities of monolayer Bi_2TeSe_2 with HSE+vdW method, respectively.

TABLE S2: Calculated elastic modulus (C^{2D}), deformation potential constant (D_l), effective mass (m_0), and mobility (μ) in x and y directions of monolayer Bi_2TeSe_2 with/without vdW at 300 K.

Bi_2TeSe_2	Strain	Direction	$C^{2D}(N/m)$	$D_l(e)$	$D_l(h)$	$m_e^*(m_0)$	$m_h^*(m_0)$	μ_e(cm^{2}V^{-1}s^{-1})	μ_h(cm^{2}V^{-1}s^{-1})
	-	x	59.94	7.17	7.75	0.0812	0.1037	2510	1317
w- vdW	-	x	61.22	7.32	8.28	0.0871	0.1029	2133	1198
	-	y	54.65	7.32	8.33	0.0812	0.1037	2195	1039
w- vdW	-	y	56.03	7.73	8.27	0.0871	0.1029	1930	1099
	-6%	x	87.23	7.13	11.61	0.0338	0.0332	21353	8316
w- vdW	-6%	x	83.54	7.15	11.54	0.0335	0.0330	20678	8181

III. ANLYSIS OF THE BAND STRUCTURES FOR MONOLAYER BI$_2$TESE$_2$

We employ the QUANTUM EXPRESSO code with both fully relativistic and scalar relativistic pseudopotentials to analyze the band structures for monolayer Bi$_2$TeSe$_2$ with and without SOC effects[3,4], as shown in Fig. S4. The irreducible representations (irreps) for energy levels near Fermi level at Γ point are obtained by the QUANTUM EXPRESSO code as well and shown in Fig. S4. The small group for Γ point is D_{3d}. The irreps for maximum of valence band and minimum of conduction band without SOC effects at Γ point are two-dimensional (2D) Γ_3^- with odd parity and one-dimensional (1D) Γ_1^+ with even parity, as shown in Fig. S4(a). The SOC effect splits the 2D Γ_3^- into degenerate 1D Γ_6^- and 1D Γ_5^-, and 2D Γ_4^- in the double-group representations, as shown in Fig. S4(b). The SOC effect also transfers the 1D Γ_1^+ into 2D Γ_4^+. Therefore, the irreps for VBM and CBM in the double-group representations are degenerate Γ_5^-&Γ_6^- and Γ_4^+ respectively, as shown in Fig. S4(b). Since the order of parities does not change when considering SOC effects, no band inversion takes place at Γ point for monolayer Bi$_2$TeSe$_2$, thus it is topologically trivial. We have further checked the topological properties for monolayer Bi$_2$TeSe$_2$ by using the state-of-art software SymTopo[5], and the calculated symmetry-based indicator is (0,0,0,0), which confirms that monolayer Bi$_2$TeSe$_2$ is a trivial insulator.

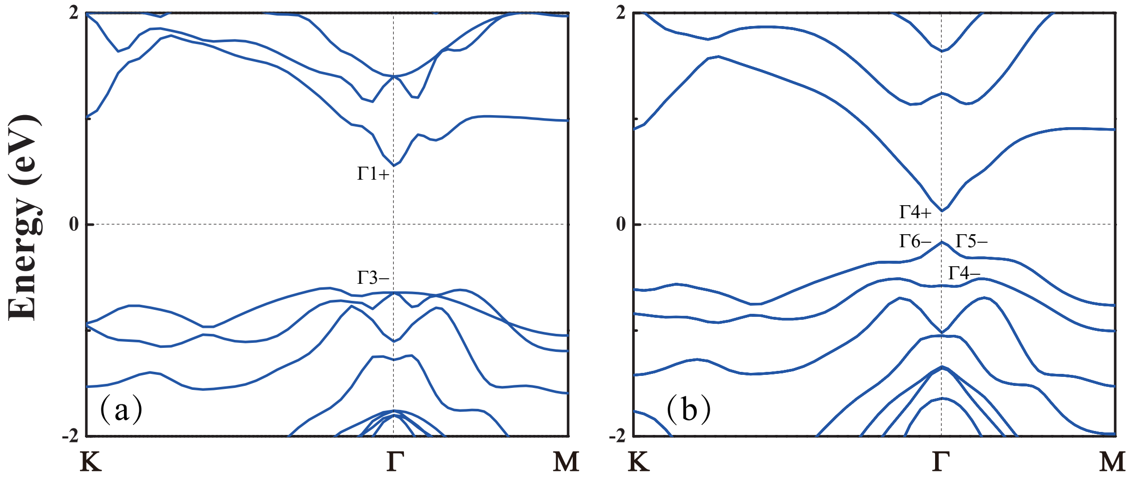

FIG. S4: Band structures for monolayer Bi$_2$TeSe$_2$ (a) without and (b) with SOC effects.

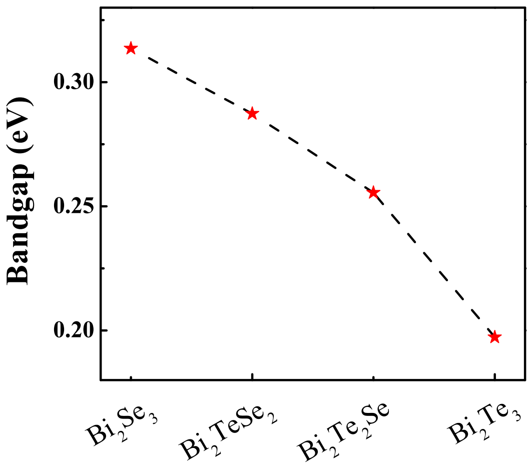

FIG. S5: Dependence of the bandgaps of Bi_2Se_3, Bi_2TeSe_2, Bi_2Te_2Se, Bi_2Se_3 on SOC strength.

IV. SOC EFFECTS ON BANDGAPS AND MOBILITIES

Since Te is below Se in the periodic table, the SOC effect of Te atom is stronger than Se atoms. As shown in Table 1, the calculated SOC strength for Te atom is 140 meV smaller than Se atom, which means that the SOC effect of heavier Te atoms is stronger than Se atoms. To further investigate influences of the SOC effects on band structures and carrier mobilities, we change the ratios of Te and Se in monolayer Bi_2TeSe_2 with fixed crystal structures by replacing Se atoms with Te atoms, and monolayers of Bi_2Se_3, Bi_2TeSe_2, Bi_2Te_2Se and Bi_2Se_3 with identical crystal structures are generated. By using first-principle method, the calculated bandgaps for the four monolayers are shown in Fig. S5, which shows that, when the Te concentration increases, the value of bandgap decreases from 1.08 eV to 0.29 eV. The decreased bandgap is resulted from the stronger SOC strength of Te atoms, considering similar chemical properties of Te and Se atoms and identical crystal structures. According to the simple two-band *kp* model shown as Eq. (12), the value of m^* increases when the value of bandgap increases. Thus, when the value of bandgap decreases with increasing concentration of Te atoms, the value of m^* increases, which finally decreases the value of carrier mobilities, according to the deformation-potential theory shown as Eq. (7).

V. CLEAVAGE ENERGY FOR BI$_2$TE$_2$SE

Fig. S6 shows the resulting cleavage energy by determining the total energy difference (per unit cell) with respect to the ground state of the fractured structure with four quintuple layers (QLs) slab as a function of distance. And the calculated cleavage energy of Bi_2TeSe_2 is 0.37 J/m^2, which confirms that monolayer Bi_2TeSe_2 could be feasible to be experimentally exfoliated from its bulk single crystals considering the weak vdW interactions between adjacent QLs.

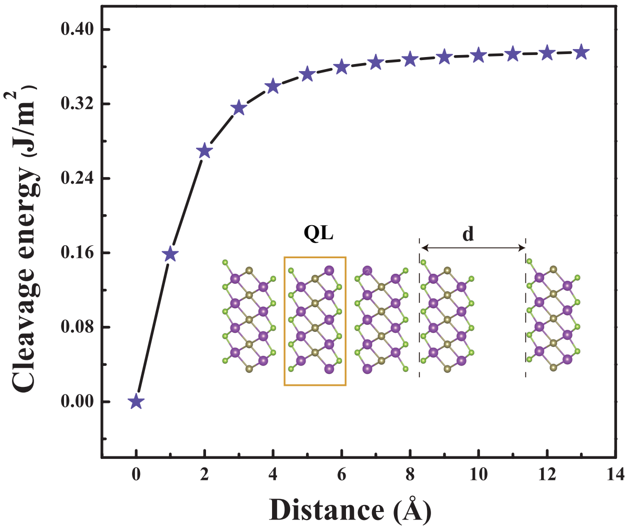

FIG. S6: Cleavage energy as a function of the distance between a top QL and the bottom three QLs of Bi_2TeSe_2. Inserted is the schematic view of the cleavage process of monolayer from the four-QLs slab of Bi_2TeSe_2.

---

[*] Electronic address: `zhangh@fudan.edu.cn`

[†] Electronic address: `zlfang@fudan.edu.cn`

[1] Y. Wang, J. Lv, L. Zhu and Y. Ma, *Phys. Rev. B*, 2010, **82**, 094116.

[2] H. Wang, Y. Wang, J. Lv, Q. Li, L. Zhang and Y. Ma, *Comp. Mater. Sci.*, 2016, **112**, 406 – 415.

[3] P. Giannozzi, S. Baroni, N. Bonini, M. Calandra, R. Car, C. Cavazzoni, D. Ceresoli, G. L. Chiarotti, M. Cococcioni, I. Dabo, A. D. Corso, S. de Gironcoli, S. Fabris, G. Fratesi, R. Gebauer, U. Gerstmann, C. Gougoussis, A. Kokalj, M. Lazzeri, L. Martin-Samos, N. Marzari, F. Mauri, R. Mazzarello, S. Paolini, A. Pasquarello, L. Paulatto, C. Sbraccia, S. Scandolo, G. Sclauzero, A. P. Seitsonen, A. Smogunov, P. Umari and R. M. Wentzcovitch, *Journal of Physics: Condensed Matter*, 2009, **21**, 395502.

[4] P. Giannozzi, O. Andreussi, T. Brumme, O. Bunau, M. B. Nardelli, M. Calandra, R. Car, C. Cavazzoni, D. Ceresoli, M. Cococcioni, N. Colonna, I. Carnimeo, A. D. Corso, S. de Gironcoli, P. Delugas, R. A. DiStasio, A. Ferretti, A. Floris, G. Fratesi, G. Fugallo, R. Gebauer, U. Gerstmann, F. Giustino, T. Gorni, J. Jia, M. Kawamura, H.-Y. Ko, A. Kokalj, E. Küçükbenli, M. Lazzeri, M. Marsili, N. Marzari, F. Mauri, N. L. Nguyen, H.-V. Nguyen, A. O. de-la Roza, L. Paulatto, S. Poncé, D. Rocca, R. Sabatini, B. Santra, M. Schlipf, A. P. Seitsonen, A. Smogunov, I. Timrov, T. Thonhauser, P. Umari, N. Vast, X. Wu and S. Baroni, *Journal of Physics: Condensed Matter*, 2017, **29**, 465901.

[5] T. Z. H. H. C. F. Z. J. Yuqing He, Yi Jiang, *Chinese Phys. B*, 2019, **28**, 87102.